Journal of Power Sources 196 (2011) 3033–3038

Contents lists available at ScienceDirect

Journal of Power Sources

journal homepage: www.elsevier.com/locate/jpowsour

Silver nanorods for oxygen reduction: Strong effects of protecting ligand on the electrocatalytic activity

Yizhong Lu[a,b], Yichen Wang[a,b], Wei Chen[a,*]

[a] State Key Laboratory of Electroanalytical Chemistry, Changchun Institute of Applied Chemistry, Chinese Academy of Sciences, Changchun, Jilin 130022, China
[b] Graduate School of the Chinese Academy of Sciences, Beijing 100039, China

ARTICLE INFO

Article history:
Received 18 October 2010
Received in revised form
16 November 2010
Accepted 22 November 2010
Available online 26 November 2010

Keywords:
Electrocatalysis
Nanorod
Oxygen reduction
Rotating disk electrode
Silver
Voltammetry

ABSTRACT

Uniform and ultralong silver nanorods are synthesized with a wet chemical reduction method by using PVP as a stabilizer. The crystal structure and morphology of the synthesized nanorods are characterized with transmission electron microscopy (TEM), powder X-ray diffraction (XRD) and UV–vis absorption spectroscopy. The electrocatalytic activity of the Ag nanorods with and without PVP stabilizer, towards oxygen reduction reaction (ORR), is studied and compared by cyclic voltammetry (CV) and rotating disk electrode (RDE) measurements in alkaline solution. Compared to the low current density and incomplete two-electron reaction process of ORR with PVP-protected Ag nanorods, the catalytic activity of the Ag nanorods with removal of the PVP is found to be enhanced remarkably with much higher oxygen reduction current density and the most efficient four-electron process.

1. Introduction

Direct liquid fuel cells, powered by hydrogen or small molecules including methanol, formic acid, have attracted much attention as a potential efficient energy source with high energy performance, low air pollution and low operating temperature [1]. To achieve the high current density and low over-potential needed for the practical commercial application, Pt, Pd and their alloys have been examined extensively as electro-catalysts for the fuels oxidation on anode and for oxygen reduction on cathode [2,3]. Over the past decades, studies on designing of new nanostructures such as shape-controlled nanoparticles, nanorod, and nanowire with unique catalytic properties have been widely studied as electrocatalysts for fuel cells [4,5]. However, due to the high cost and limited reserves of platinum-group metals (Pt, Pd), numerous studies have focused on the non-platinum electrocatalysts such as transition metal oxides [6–8], transition metal sulfides [9], transition metal macrocyclic complexes [10,11], and metal-containing porphyrin systems [12].

Bulk gold and silver attract little attention as cathode electrocatalysts due to the poor catalytic activity compared to the Pt- and Pd-based materials. The poor activity of coin metals (Au, Ag and Cu) is usually attributed to its filled d bands, resulting in the higher activation barriers than those created for other transition metals with only partially filled d bands [13,14]. However, gold clusters were found to be highly reactive at room temperature and the reactivity depends on the electrical charge (positive, neutral or negative) and the atomic number of clusters [13]. For instance, highly dispersed gold nanoparticles display unexpectedly high catalytic activities in many important chemical reactions such as hydrogenation of acrolein [15], selective hydrosilylation [16], cyclopropanation of alkenes [17], low temperature CO and H_2 oxidation [18], and NO reduction [19]. More recently, Herzing et al. [20] observed high catalytic activity in CO oxidation with gold clusters containing only ~10 gold atoms (~0.5 nm in diameter). In electrocatalysis studies [21], a series of gold nanoclusters with core size smaller than 2 nm (0.8–1.7 nm) were synthesized and the electrocatalytic activity towards oxygen reduction was investigated in alkaline media to evaluate the size effect on the electrocatalytic activity. It was found that the sub-nanometer sized Au particles exhibited high activity for oxygen reduction and the electrocatalytic activity of Au cluster for oxygen reduction is strongly dependent on the core size of the clusters.

Recently, silver nanoparticles were also studied as cathode electrocatalysts for oxygen or hydrogen peroxide reduction [22–25]. It was found that the oxygen reduction reaction (ORR) with the Ag island has the efficient four-electron reduction of adsorbed oxygen to water [22]. In the study of peroxide reduction at silver nanoparticle array, the catalytic performance varies with the diameter of the Ag nanoparticles [25]. The unusual catalytic activ-

* Corresponding author. Tel.: +86 431 85262061; fax: +86 431 85262697.
E-mail address: weichen@ciac.jl.cn (W. Chen).

0378-7753/$ – see front matter © 2010 Elsevier B.V. All rights reserved.
doi:10.1016/j.jpowsour.2010.11.119

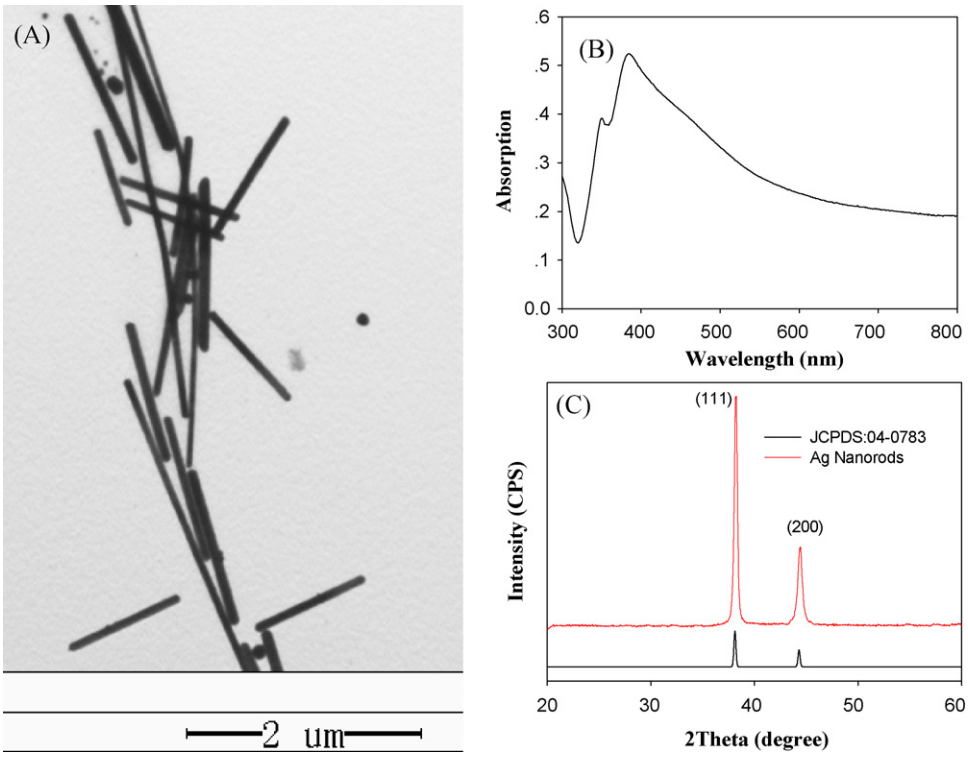

Fig. 1. (A) Transmission electron micrograph (TEM), (B) UV–vis absorption spectrum and (C) X-ray diffraction (XRD) of the synthesized silver nanorods. In UV–vis spectrum collection, ~0.1 mg mL^{-1} silver nanorods were dispersed in pure water. For comparison, the Joint Committee Powder Diffraction Standard (JCPDS) No. 04-0783 of silver was included in the XRD patterns.

ity of gold and silver nanoparticles may be accounted for by the high fraction of surface atoms and their low coordination numbers, which may be manipulated readily by the nanoparticle dimensions. From the previous investigations of the ORR with Au and Ag nanoparticle catalysts, one can see that the Au and Ag materials on nano-scale have remarkable activity in comparison with the inert catalytic properties of the bulk ones. However, most of these earlier studies focused on the nanoparticles. The electrocatalytic activities of one-dimensional coin metal nanomaterials, such as nanorods, nanowires, nanotubes, and the stabilizer effects on the reaction kinetic of oxygen reduction are still scarce.

In the present report, Ag nanorods stabilized by PVP were firstly synthesized with polyol process and then the PVP was removed by ligand exchange with hexanethiol. The surface clean Ag nanorods were finally obtained by removal of the hexanethiol with plasma cleaner. The catalytic activity of the PVP-protected and the surfactant-free Ag nanorods towards ORR was studied in detail. The results showed that the Ag nanowire exhibits efficient catalytic activity and the protecting ligands strongly reduce the electrocatalytic activity. The present study shows that the Ag nanowire may be used as a powerful cathode electrocatalyst for oxygen reduction.

2. Experimental

2.1. Materials

Silver nitrate ($AgNO_3$, ≥99.8%, Beijing Chemical Reagent), poly(vinyl pyrrolidone) (PVP, Mw ≈ 55,000, Aldrich), ethylene glycol (EG, A.R. grade, Beijing Chemical Reagent), potassium hydroxide (KOH, ACROS), sodium chloride (NaCl, ≥99.5%, Beijing Chemical Reagent), and 1-hexanethiol (C_6SH, 95%, Aldrich) were used as received. Water was supplied by a Water Purifier system (18.3 MΩ cm). Ultrapure N_2 and O_2 were used for the deaeration and oxygen reduction reaction, respectively.

2.2. Synthesis of silver nanorods

The Ag nanorods were synthesized according to the modified procedures described before [26,27]. In a typical reaction, 200 mM of PVP dissolved in 10 ml of ethylene glycol was refluxed at 160 °C for 1 h under vigorous stirring. 5 mL of a freshly prepared $AgNO_3$ solution (0.15 M in EG) was then added in a dropwise fashion into the solution. The reaction mixture was stirred for another 60 min at 160 °C. After the solution was cooled to room temperature, the final dispersion was diluted with ethanol in a ratio of 1:10 and then centrifuged at a rate of 2000 rpm for 20 min. The nanorods were collected and redispersed in ethanol. This process was repeated about 4 times. The PVP-stabilized Ag nanorods were finally dispersed in ethanol for the further experiments. Such Ag nanorods were denoted as Ag-PVP.

Ligand exchange of Ag-PVP with 1-hexanethiol (C_6SH) was carried out by mixing PVP-stabilized Ag nanorods and 1-hexanethiol with the molar ratio of 1:3 in ethanol under magnetic stirring. After about 12 h, it can be seen that a layer of Ag nanorods was dispersed on the ethanol surface, suggesting the hydrophobic surface properties of the nanorods functionalized with C_6SH protecting ligands. The products were collected and washed with ethanol to remove excessive C_6SH and displaced PVP. The purified Ag nanorods were dispersed in dichloromethane (DCM). The Ag nanorods functionalized with C_6SH were denoted as Ag-C_6SH.

2.3. Electrochemistry

Prior to the deposition of the Ag nanorods onto an electrode surface for electrocatalytic assessment, a glassy carbon (GC) electrode (3.0 mm diameter) was polished with alumina slurries (5, 1 and 0.5 μm) and cleansed by sonication in 0.1 M HNO_3, H_2SO_4 and nanopure water for 10 min successively. 10 μL of the Ag-C_6SH nanorods in DCM (1 mg mL^{-1}) was then dropcast onto the clean GC

electrode surface by a Hamilton microliter syringe and was dried by a gentle nitrogen flow for ca. 2 min. The C_6SH ligands were then removed by Plasma cleaner (PDC-32G, Harrick Plasma, US) treatment for 20 min. The electrode was then rinsed with nanopure water and ethanol to remove the impurities. The resulting clean electrode was denoted as Ag/GC.

To study the effect of PVP on the electrocatalytic activity of Ag nanorods, 1 mg of the Ag-PVP nanorods was dispersed ultrasonically in 1 mL pure water and 80 μL 5 wt% Nafion solution. After the ink formed homogeneously, 10 μL of the catalyst ink was then dropped on the GC electrode with a micropipette and then dried in air. The working electrodes were denoted as Ag-PVP/GC.

Voltammetric measurements were carried out with a CHI 750D electrochemical workstation. The Ag/GC and Ag-PVP/GC electrodes prepared above were used as the working electrodes. An Ag/AgCl (in 3 M NaCl, aq.) and a Pt coil were used as the reference and counter electrodes, respectively. All electrode potentials in the present study were referred to this Ag/AgCl reference. Cyclic voltammetry and rotating disk voltammetry were carried out in 0.1 M KOH electrolyte by using a computer-controlled CHI 750D electrochemical workstation. The rotating disk voltammograms on all electrodes were measured at the potential scan rate of 20 mV s^{-1}. Oxygen reductions were examined by first bubbling the electrolyte solution with ultrahigh purity oxygen for at least 15 min and then blanketing the solution with an oxygen atmosphere during the entire experimental procedure. All electrochemical experiments were carried out at room temperature.

2.4. Material characterizations

UV–vis spectroscopic studies were performed with a Cary spectrometer using a 1-cm quartz cuvette with a resolution of 2 nm. Powder X-ray diffraction (XRD) was performed on a PW1700 Powder Diffractometer using Cu-Kα radiation with a Ni filter (λ = 0.154059 nm at 30 kV and 15 mA). The morphology and crystal structure of the Ag nanorods were measured with Hitachi H-600 transmission electron microscopy (TEM) operated at 100 kV.

3. Results and discussion

3.1. Structural characterizations

Fig. 1A displays the representative TEM micrograph of the synthesized silver nanorods. It can be seen that the resulting Ag nanorods are very uniform in both shape and size. The average diameter is 83 ± 3 nm with aspect ratio of 14.5 ± 4.4. Fig. 1B shows the UV–vis absorption spectrum of the Ag nanorods in nanopure water. Two absorption bands at about 350 and 385 nm were observed, which are attributed to the surface plasmon resonance bands of the longitudinal and transverse modes of the silver nanorods, respectively. Such UV–vis absorption features agree well with those obtained with silver nanowire and nanorods in the previous reports [28–30]. To examine the crystalline structure of the resulting nanorods, powder X-ray diffraction measurements were also carried out. Fig. 1C shows the XRD patterns of the nanorods and the JCPDS data of silver. Two strong diffraction peaks are ascribed to the (1 1 1) and (2 0 0) planes of metallic silver, which are in excellent agreement with the face-centered cubic (fcc) structure of silver in JCPDS (NO.04-0783).

3.2. Cyclic voltammetry

The electrocatalytic activity of the silver nanorods towards oxygen reduction was then examined by cyclic voltammetry (CV). The electrodes prepared from PVP-protected and the surfactant-free Ag nanorods were denoted as Ag-PVP/GC and Ag/GC, respectively.

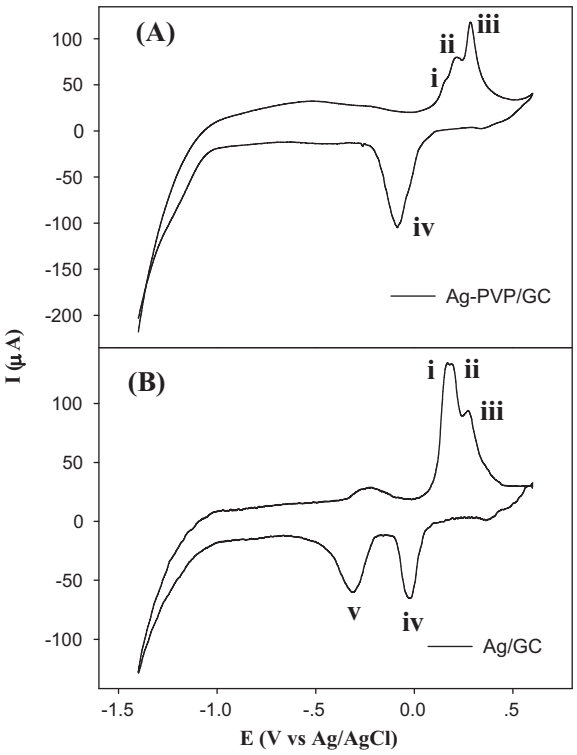

Fig. 2. Cyclic voltammograms of the Ag-PVP/GC (A) and Ag/GC (B) electrodes in N_2-saturated 0.1 M KOH solution. Potential scan rate 0.1 V s^{-1}.

Fig. 2 shows the representative CVs of Ag-PVP/GC (Fig. 2A) and Ag/GC (Fig. 2B) in 0.1 M KOH that was saturated with N_2 at a potential sweep rate of 0.1 V s^{-1}. From the CV of Ag-PVP/GC within the potential range of −1.4 to 0.6 V (vs Ag/AgCl), three anodic current peaks were clearly observed at +0.15, +0.21 and +0.28 V, respectively. The small peak (i) could be attributed to the formation of a few monolayers of AgOH and Ag(I) species. The peaks (ii) and (iii) were attributed to the formation of inner hydrous oxide layer and more compact outer oxide layer, respectively. In the reverse potential scan, the cathodic current peak at −0.086 V (peak (iv)) was ascribed to the electroreduction of the silver oxides formed during the anodic potential scan. The observed CV feature is very similar to that from polycrystalline Ag electrodes reported previously [31–33]. From the CV of the Ag/GC in the same potential window shown in Fig. 2B, the anodic current peaks corresponding to the formation of silver oxides at +0.165 (i), +0.193 (ii) and +0.274 V (iii), and the reduction peak at −0.023 V (peak (iv)) during the cathodic potential scan can also be observed. Compared to the CV of Ag-PVP/GC electrode, one more cathodic peak at −0.31 V (peak (v)) was observed at Ag/GC. Such voltammetric behavior was also observed at silver oxide electrodes [33]. In the present study, with the PVP removal, silver oxide layers maybe more easily formed at the surface of the nanorods in comparison with the very stable surface of PVP-stabilized Ag nanorods. Moreover, the potential for Ag oxides reduction on Ag/GC electrode negatively shifts to −0.023 V from −0.086 V obtained on Ag-PVP/GC electrode. The different CV features observed at Ag-PVP/GC and Ag/GC electrodes suggest that the plasma clean treatment affects the electrochemical behaviors of the Ag nanorods.

Fig. 3 shows the cyclic voltammograms (CVs) of the Ag/GC and Ag-PVP/GC electrodes in an aqueous solution of 0.1 M KOH which was saturated with nitrogen or oxygen at a potential scan rate of 0.1 V s^{-1}. Note that the voltammetric currents have been normalized to the real active surface areas (i.e., electrochemically active

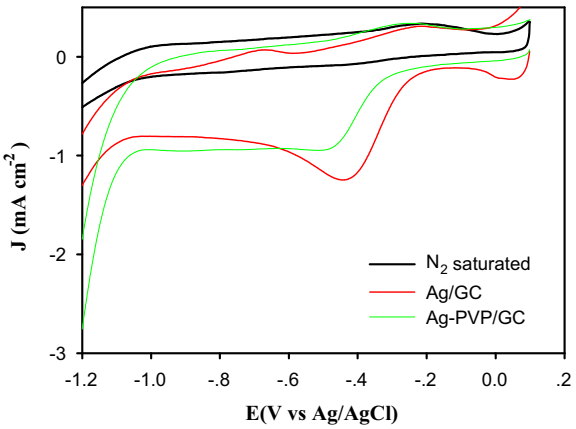

Fig. 3. Cyclic voltammograms of the PVP-stabilized (Ag-PVP/GC) and PVP-free (Ag/GC) silver nanorods electrodes in 0.1 M KOH saturated with oxygen and of the Ag/GC electrode in N_2-saturated 0.1 M KOH solution. Potential scan rate 0.1 V s^{-1}.

surface areas) of the respective electrodes which are calculated according to the oxygen adsorption measurement method proposed by Trasatti and Petrii [34]. Some voltammetric features in Fig. 3 should be noted. First, from the CV of Ag/GC electrode in the N_2-saturated solution (black curve), the voltammetric currents were featureless within the potential range of −1.2 to +0.1 V. In contrast, when the electrolyte solution was saturated with O_2, obvious reduction currents with well-defined cathodic peaks around −0.4 V can be seen clearly on the both Ag/GC and Ag-PVP/GC electrodes, indicating the high electrocatalytic activity of the synthesized silver nanorods towards oxygen reduction. It should be noted that the potential window different from Fig. 2 was used in Fig. 3. From Fig. 2, it can be seen that the formation of silver oxides occurs mainly at potentials more positive than +0.1 V. In order to avoid the interference of silver oxide reduction on oxygen molecules reduction, narrow potential window (−1.2 to +0.1 V) was applied in the studies of oxygen reduction reaction (Fig. 3). From the black curve in Fig. 3, no obvious reduction current was observed from the reduction of silver oxides. Since there is no reduction current from silver oxides (black curve), we anticipate that the reduction current peaks shown in Fig. 3 come directly from the oxygen reduction. Second, the current density and onset potentials, the most two important parameters to evaluate the activity of electrocatalysts, are much different for Ag/GC and Ag-PVP/GC electrodes. Take the case of cathodic peak of oxygen reduction, for PVP-passivated Ag nanorods (green curve), the peak current density and the peak potential were found to be approximately −0.95 mA cm^{-2} and 0.52 V, respectively. However, for the surface-cleaned Ag nanorods (red curve), the peak current density increased to −1.25 mA cm^{-2}, and the peak potential shifted positively to −0.44 V. Larger current density and more positive onset potential were obtained with Ag/GC in comparison with Ag-PVP/GC electrode. Moreover, from the CV of Ag-PVP/GC, two oxygen reduction peaks can be observed at around −0.52 and −0.91 V, but only one current peak appeared for Ag/GC electrode at −0.44 V. Such voltammetric features suggest strongly that efficient four-electron reaction occurred for oxygen reduction on Ag nanorods with naked surface, but less efficient pathway involves two steps occurred on PVP-protected Ag nanorods. All the voltammetric studies showed clearly that the Ag nanorods with naked surface exhibit much better electrocatalytic activity for ORR than those capped with stabilizer (PVP). By comparing the current density and onset potential of oxygen reduction, the electrocatalytic activity of the present silver nanorods was found to be comparable to that of supported gold nanocluster electrocatalysts [8].

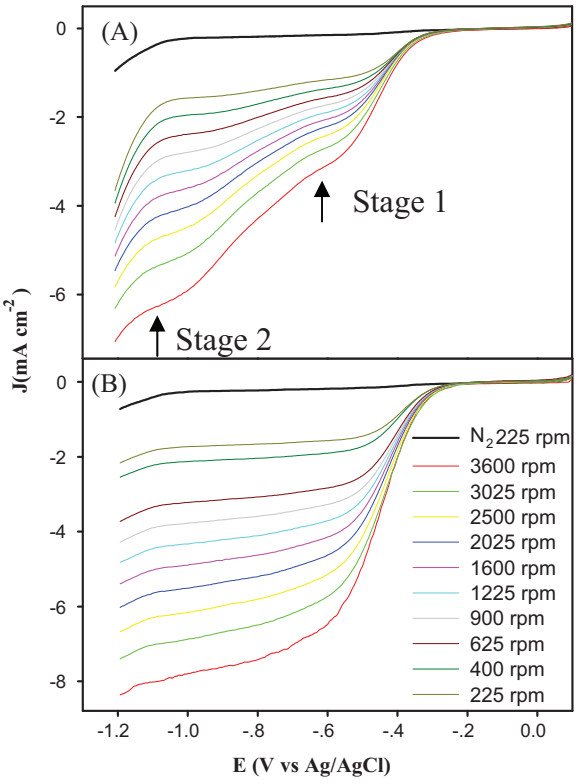

Fig. 4. Rotating-disk voltammograms recorded on Ag-PVP/GC (A) and Ag/GC (B) in 0.1 M KOH saturated with oxygen at different rotation rates (shown as figure legends). DC ramp 20 mV s^{-1}.

3.3. Rotating disk voltammetry

To further examine the electrocatalytic activity, the reaction kinetic of oxygen reduction at the PVP-passivated and naked Ag nanorods were also studied with rotating disk voltammetry. Fig. 4 shows a series of rotating disk voltammograms (RDVs) of ORR recorded at Ag-PVP/GC (Fig. 4A) and Ag/GC (Fig. 4B) in an oxygen-saturated 0.1 M KOH solution at different rotation rates (from 225 to 3600 rpm). For the ORR on Ag-PVP/GC shown in Fig. 4A, two stages of limiting current can be observed at around −0.6 and −1.0 V, respectively, suggesting electrocatalytic reduction of oxygen proceeds via two-step processes:

$$O_{2(ad)} + H_2O + 2e^- \rightarrow HO_2^- + OH^- \quad (1a)$$

$$HO_2^- + H_2O + 2e^- \rightarrow 3OH^- \quad (1b)$$

From the RDV at 3600 rpm, it can be seen that the current density at stage 2 is nearly twice that of the first stage, suggesting that if the first stage is a two-electron process, the reaction occurred at the second stage should be an overall four-electron process. However, from the RDVs of oxygen reduction recorded at Ag/GC electrode (Fig. 4B), one can see that there is only one stage with much better defined current density plateaus than those obtained at Ag-PVP nanorods (Fig. 4A) and other non-platinum nano-electrocatalysts. In addition, the limiting current density at each rotation rate is larger than that of the second plateau obtained from Ag-PVP/GC. Such RDV features indicate that the ORR on stabilizer-free Ag nanorods proceeds via the most efficient four-electron process:

$$O_{2(ad)} + 2H_2O + 4e^- \rightarrow 4OH \quad (2)$$

The voltammetric results from rotating disk electrodes (RDEs) strongly indicated that the stabilizers (PVP) on the Ag nanorods surface evidently reduce the electrocatalytic activity towards oxygen reduction.

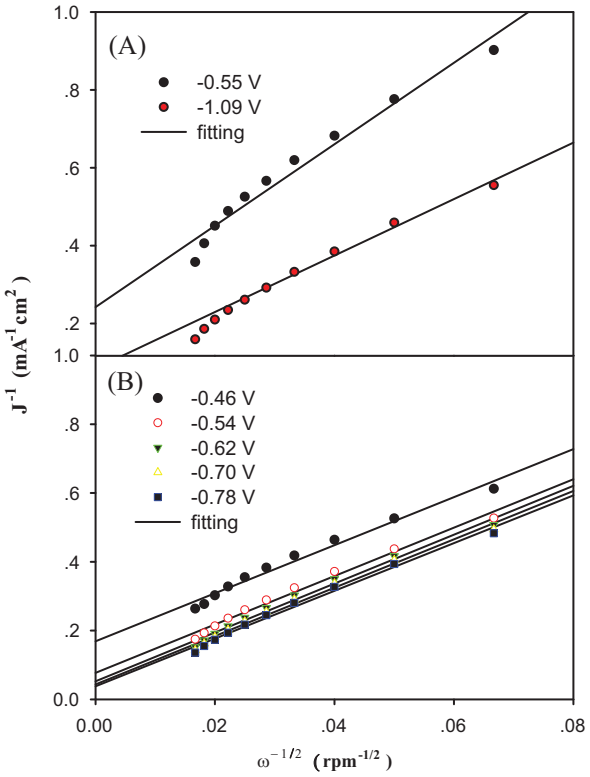

Fig. 5. Koutecky–Levich plots (J^{-1} vs $\omega^{-1/2}$) for Ag-PVP/GC (A) and Ag/GC (B) at different potentials (shown as figure legends). Symbols are experimental data obtained from the corresponding rotating-disk voltammograms shown in Fig. 4. Lines are the linear regressions.

Fig. 5A depicts the Koutecky–Levich plots (J^{-1} vs $\omega^{-1/2}$) of Ag-PVP/GC electrode at potentials of −0.55 and −1.09 V, corresponding to the first and second stages, respectively (shown in Fig. 4A). The kinetic parameters can be analyzed with the Koutecky–Levich equations [Eqs. (3)–(5)]:

$$\frac{1}{J} = \frac{1}{J_K} + \frac{1}{J_L} = \frac{1}{J_K} + \frac{1}{B\omega^{1/2}} \quad (3)$$

$$B = 0.62nFC_O D_O^{2/3} \nu^{-1/6} \quad (4)$$

$$J_K = nFkC_O \quad (5)$$

where J is the measured current density, J_K and J_L are the kinetic and diffusion limiting current density, respectively, ω is the electrode rotation rate, n is the overall number of electron transferred, F is the Faraday constant, C_O is the bulk concentration of O_2 dissolved in the electrolyte, D_O is the diffusion coefficient for O_2, ν is the kinematic viscosity of the electrolyte, and k is the electron transfer rate constant. According to Eqs. (3) and (4), the number of electrons transferred and J_K can be obtained from the slope and intercept of the Koutecky–Levich plots, respectively. The numbers of electrons transferred were calculated to be 2.6 and 3.8 (≈4) for ORR on Ag-PVP/GC electrode at the first and second stages, respectively, by using the literature values for $C_O = 1.2 \times 10^{-3}$ mol L^{-1} [35], $D_O = 1.9 \times 10^{-5}$ cm^2 s^{-1} [35] and $\nu = 0.01$ cm^2 s^{-1} [36] in 0.1 M KOH. The kinetic limiting current density (J_K) was estimated to be −4.17 and −11.76 mA cm^{-2} at −0.55 V and −1.09 V, respectively. The kinetic results showed that oxygen electro-oxidation on PVP-protected Ag nanorods involve two successive two-electron processes, which agrees well with the CV and RDE results. Fig. 5B shows the corresponding Koutecky–Levich plots of ORR obtained on Ag/GC electrode at various potentials. It can be seen that the slopes remain approximately constant over the potentials range from −0.46 to −0.78 V, indicating consistent numbers of electron transfer for ORR at different electrode potentials. From the slopes of the Koutecky–Levich plots, the numbers of electrons transferred were determined to be 3.9 (≈4) for ORR on Ag/GC. The kinetic limiting current density was calculated to be −13 mA cm^{-2} at −0.54 V, which is much larger than those obtained on Ag-PVP/GC electrode at both −0.55 V and −1.09 V. By comparing the CV and RDE results on Ag-PVP/GC and Ag/GC electrodes, it is obvious that the oxygen electro-reduction proceeds by the incomplete pathway on the Ag nanorods passivated with PVP, where the two-electron reaction route was favoured, whereas efficient four-electron reaction pathway occurred after PVP was removed from the surface of Ag nanorods. The significant difference indicates that the catalytic activity of Ag nanorods is greatly reduced by the PVP which interacts strongly with the Ag surface and to blocks the most of the active sites. After PVP removed, the active sites on Ag nanorod surface are released for O_2 adsorption, leading to the enhanced electrocatalytic activity for ORR.

4. Conclusions

In the present study, we synthesized uniform and ultralong silver nanorods with a wet chemical method by using PVP as the surface stabilizer. The effect of PVP on the electrocatalytic activity of Ag nanorods towards oxygen-reduction was examined with electrochemical cyclic and rotating disk voltammetric measurements. The results showed that the PVP on the Ag nanorod surface reduces heavily the electrocatlytic activity. The catalytic activity of the Ag nanorods is enhanced remarkably by removing the PVP with much higher oxygen reduction current density and the most efficient four-electron process in comparison with the low current density and incomplete two-electron reaction process. Due to the high electrocatalytic activity towards ORR, protecting ligand-free Ag nanorods may be a promising cathode electrocatalyst for fuel cells.

Acknowledgment

This work was supported by the startup funds for scientific research, Changchun Institute of Applied Chemistry, Chinese Academy of Sciences.

References

[1] B.C.H. Steele, A. Heinzel, Nature 414 (2001) 345.
[2] V.R. Stamenkovic, B.S. Mun, M. Arenz, K.J.J. Mayrhofer, C.A. Lucas, G.F. Wang, P.N. Ross, N.M. Markovic, Nature Materials 6 (2007) 241.
[3] W. Chen, J.M. Kim, S.H. Sun, S.W. Chen, Journal of Physical Chemistry C 112 (2008) 3891.
[4] Y. Xia, Y.J. Xiong, B. Lim, S.E. Skrabalak, Angewandte Chemie-International Edition 48 (2009) 60.
[5] A.C. Chen, P. Holt-Hindle, Chemical Reviews 110 (2010) 3767.
[6] Y. Liu, A. Ishihara, S. Mitsushima, N. Kamiya, K. Ota, Journal of the Electrochemical Society 154 (2007) B664.
[7] S.V. Mentus, Electrochimica Acta 50 (2004) 27.
[8] W. Chen, D. Ny, S.W. Chen, Journal of Power Sources 195 (2010) 412.
[9] R.W. Reeve, P.A. Christensen, A. Hamnett, S.A. Haydock, S.C. Roy, Journal of the Electrochemical Society 145 (1998) 3463.
[10] H.S. Liu, C.J. Song, Y.H. Tang, J.L. Zhang, H.J. Zhang, Electrochimica Acta 52 (2007) 4532.
[11] L. Zhang, J.J. Zhang, D.P. Wilkinson, H.J. Wang, Journal of Power Sources 156 (2006) 171.
[12] R. Holze, I. Vogel, W. Vielstich, Journal of the Electrochemical Society 133 (1986) C115.
[13] D.M. Cox, R. Brickman, K. Creegan, A. Kaldor, Zeitschrift Fur Physik D-Atoms Molecules and Clusters 19 (1991) 353.
[14] P. Madhavan, J.L. Whitten, Journal of Chemical Physics 77 (1982) 2673.
[15] P. Claus, A. Bruckner, C. Mohr, H. Hofmeister, Journal of the American Chemical Society 122 (2000) 11430.
[16] A. Corma, C. Gonzalez-Arellano, M. Iglesias, F. Sanchez, Angewandte Chemie-International Edition 46 (2007) 7820.

[17] A. Corma, I. Dominguez, T. Rodenas, M.J. Sabater, Journal of Catalysis 259 (2008) 26.
[18] G.C. Bond, D.T. Thompson, Catalysis Reviews-Science and Engineering 41 (1999) 319.
[19] M. Haruta, Catalysis Today 36 (1997) 153.
[20] A.A. Herzing, C.J. Kiely, A.F. Carley, P. Landon, G.J. Hutchings, Science 321 (2008) 1331.
[21] W. Chen, S.W. Chen, Angewandte Chemie-International Edition 48 (2009) 4386.
[22] A. Kongkanand, S. Kuwabata, Electrochemistry Communications 5 (2003) 133.
[23] H.K. Lee, J.P. Shim, M.J. Shim, S.W. Kim, J.S. Lee, Materials Chemistry and Physics 45 (1996) 238.
[24] L. Demarconnay, C. Coutanceau, J.M. Leger, Electrochimica Acta 49 (2004) 4513.
[25] F.W. Campbell, S.R. Belding, R. Baron, L. Xiao, R.G. Compton, Journal of Physical Chemistry C 113 (2009) 9053.
[26] Y.G. Sun, Z.L. Tao, J. Chen, T. Herricks, Y.N. Xia, Journal of the American Chemical Society 126 (2004) 5940.
[27] A. Tao, F. Kim, C. Hess, J. Goldberger, R.R. He, Y.G. Sun, Y.N. Xia, P.D. Yang, Nano Letters 3 (2003) 1229.
[28] Y.P. Bi, H.Y. Hu, G.X. Lu, Chemical Communications 46 (2010) 598.
[29] Y.G. Sun, B. Gates, B. Mayers, Y.N. Xia, Nano Letters 2 (2002) 165.
[30] Y.G. Sun, B. Mayers, T. Herricks, Y.N. Xia, Nano Letters 3 (2003) 955.
[31] M.L. Teijelo, J.R. Vilche, A.J. Arvia, Journal of Electroanalytical Chemistry 131 (1982) 331.
[32] M.L. Teijelo, J.R. Vilche, A.J. Arvia, Journal of Electroanalytical Chemistry 162 (1984) 207.
[33] M.L. Teijelo, J.R. Vilche, A.J. Arvia, Journal of Applied Electrochemistry 18 (1988) 691.
[34] S. Trasatti, O.A. Petrii, Pure and Applied Chemistry 63 (1991) 711.
[35] R.E. Davis, G.L. Horvath, C.W. Tobias, Electrochimica Acta 12 (1967) 287.
[36] A. Sarapuu, M. Nurmik, H. Mandar, A. Rosental, T. Laaksonen, K. Kontturi, D.J. Schiffrin, K. Tammeveski, Journal of Electroanalytical Chemistry 612 (2008) 78.